

Quantum bistability at the interplay between collective and individual decay

Nikita Leppenen and Ephraim Shahmoon

Department of Chemical & Biological Physics, Weizmann Institute of Science, Rehovot 7610001, Israel

We study driven collective radiation of an ensemble of atoms placed inside a cavity, accounting for individual-atom emission to free space modes. We find that the steady state exhibits a dissipative phase transition, formed by a mixture of two collective quantum states corresponding to a bistable mean-field solution. One of these states is entangled and closely resembles a coherently radiating spin state (CRSS) – the solution obtained by neglecting individual decay (Dicke superradiance) – allowing us to analytically find the optimally achievable spin squeezing. We predict quantum switching between the two states, verified by quantum trajectories simulations. The switching rate tends to vanish with the atom number, as the Liouvillian gap closes. Remarkably, this suggests that the system may reside in an entangled CRSS-like state associated with correlated Dicke physics, even in the presence of decorrelating individual decay. This opens a path for a systematic study of the interplay between collective and individual decay, in both experiments and theory.

Collective radiation is formed by the multiple scattering of photons between atom-like emitters. While this fundamental many-body problem emerges in a variety of systems and applications in quantum science and beyond [1–20], it is still far from being fully understood. The essence of collective effects in radiation is captured by the iconic Dicke superradiance model, wherein the many atoms are uniformly coupled to the radiation field [21]. The resulting indistinguishability symmetry offers an immense simplification whereby the many atoms behave as a single collective dipole and exhibit purely collective dissipation in the form of superradiance. Adding a laser that drives the atoms results in the driven Dicke model, accounting for purely collective driven-dissipative physics. Its steady state is predicted to be a coherently radiating spin state (CRSS) [22]: an entangled collective state exhibiting a phase transition [23–27] and spin squeezing [28–31].

Nevertheless, any realistic system may exhibit additional dissipative processes at the individual-constituent level, even when collective dissipation is dominant. In superradiance, this comes about by a non-uniform coupling of atoms to multiple photon modes, as typical of various platforms of quantum science, such as atom arrays [32–46] and ensembles [15, 47–49]. The resulting breakdown of the indistinguishability symmetry significantly complicates the analysis, especially when the channels of collective and individual dissipation are hard to tell apart [1–5, 30, 50–52]. Understanding superradiance in realistic systems thus calls for a systematic study of the interplay between collective and individual decay.

Here, we study a model which exhibits this interplay, and that is simple and relevant; namely, the realistic model of laser-driven atoms inside a cavity, describing typical superradiant platforms [Fig. 1(a)] [6–9]. The two competing decay processes are clearly distinguished in this case, as they result from radiation to different well-defined channels: individual-atom emission off the cavity axis, and collective radiation via the cavity mirrors. Going beyond previous mean-field [23, 24] and transient-time [53] studies, we perform a complete quantum analysis of the problem in steady-state using a combination

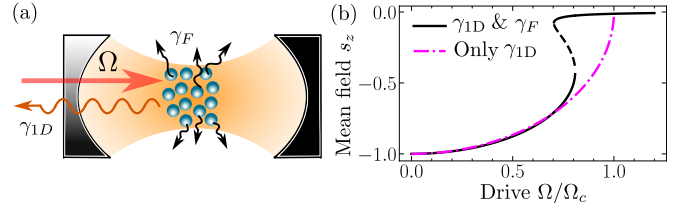


FIG. 1. (a) Atoms trapped inside an optical cavity and coherently driven by a laser amplitude Ω . The N atoms decay collectively through the cavity mirror with rate γ_{1D} and individually to off-axis modes at rate γ_F . (b) Mean-field solution of the population inversion per atom s_z from Eq. (2) (solid and dashed curve for stable and unstable solutions), with $\Omega_c = \Gamma/4$ and taking $\Gamma/\gamma = \gamma_{1D}(N-1)/(\gamma_{1D} + \gamma_F) = 15$. Dicke case (no γ_F) is plotted for reference (dash-dotted).

of numerical and analytical approaches. We find a dissipative first-order phase transition as a function of the drive strength characterized by a bimodal density matrix comprised of two states, and the dynamical switching between these states via quantum jumps. One of these states is close to a spin-squeezed CRSS, revealing the emergence of collective Dicke physics in the presence of individual-atom dissipation. We discuss the relevance of these findings for the interpretation of experiments.

Model.— We consider N identical two-level atoms placed inside a resonant optical cavity. Assuming all atoms are identically coupled to the cavity mode (e.g. laser-trapped at its antinodes [6]), and considering a fast-decaying cavity, we adiabatically eliminate the cavity mode, obtaining the master equation for the many-atom density matrix ρ [54],

$$\begin{aligned} \dot{\rho} = & -2i\Omega[\hat{S}_x, \rho] + \frac{\gamma_{1D}}{2} \left(2\hat{S}_- \rho \hat{S}_+ - \rho \hat{S}_+ \hat{S}_- - \hat{S}_+ \hat{S}_- \rho \right) \\ & + \frac{\gamma_F}{2} \sum_{n=1}^N (2\hat{\sigma}_n \rho \hat{\sigma}_n^\dagger - \rho \hat{\sigma}_n^\dagger \hat{\sigma}_n - \hat{\sigma}_n^\dagger \hat{\sigma}_n \rho) \equiv -\mathcal{L}\rho. \end{aligned} \quad (1)$$

The first term describes driving of the atoms by a resonant laser with effective Rabi frequency Ω , whereas the second term accounts for collective decay via the cavity

mode at the Purcell-enhanced rate γ_{1D} . Here $\hat{S}_- = \hat{S}_+^\dagger = \sum_{n=1}^N \hat{\sigma}_n$ is the atomic collective-spin lowering operator, with $\hat{\sigma}_n$ being the pseudo-spin lowering operator of a single atom $n \in \{1, \dots, N\}$, and $\hat{S}_{x,y,z} = 1/2 \sum_{n=1}^N \hat{\sigma}_n^{x,y,z}$. The last term accounts for additional decay of the atoms to off-axis modes outside the cavity: assuming interatomic separations exceeding the optical wavelength, the atoms appear distinguishable to these modes. This effectively leads to individual decay at the free-space spontaneous emission rate γ_F , described by individual-atom operators $\hat{\sigma}_n$.

Mean-field results.— Before we turn to a full quantum treatment, it is instructive to perform a mean-field analysis of Eq. (1). At long times, the individual decay decorrelates different atoms, which are nonetheless statistically equivalent. This motivates to use an individual factorization approximation with identical mean-field values for different atoms [23]: $\langle \hat{\sigma}_n \rangle_{\text{MF}} = s$, $\langle \hat{\sigma}_n^z \rangle_{\text{MF}} = s_z$ and $\langle \hat{\sigma}_n^\dagger \hat{\sigma}_m \rangle_{\text{MF}} = |s|^2$ for $n \neq m$. We analyze the resulting mean-field dynamical equations [54], finding their steady state as the solution of the cubic equation

$$\begin{aligned} (1 + s_z)(\gamma - s_z \Gamma)^2 + 8s_z \Omega^2 &= 0, \\ \gamma &= \gamma_F + \gamma_{1D}, \quad \Gamma = (N - 1)\gamma_{1D}, \end{aligned} \quad (2)$$

with γ and Γ forming the relevant mean-field parameters and Ω taken real.

For $\Gamma > 8\gamma$ there always exists a region of Ω values wherein Eq. (2) has two stable (and one unstable) solutions. This bistable region is seen in Fig. 1(b) by the numerical solution of Eq. (2). In the regime $\Gamma \gg \gamma$ where collective effects are dominant, we also solved Eq. (2) analytically up to third order in $\gamma/\Gamma \ll 1$ [54], with the lowest order solution recovering the result [24]

$$s_z^{(b)} = -\frac{1}{2} \mp \frac{1}{2} \sqrt{1 - \frac{2\Omega^2}{\Omega_c^2}}, \quad s_z^{(c)} = 0, \quad \Omega_c = \frac{\Gamma}{4}, \quad (3)$$

exhibiting the bistability region $0 < \Omega < \Omega_c/\sqrt{2}$.

Notably, this bistable behavior is in contrast to the Dicke case $\gamma_F = 0$, where mean-field is performed in collective variables such that correlations are retained: there, a second-order transition is obtained, $s_z = -\sqrt{1 - (\Omega/\Omega_c)^2}$ [23, 29, 31], as seen in Fig. 1(b). However, for $\gamma_F \neq 0$ and long enough times, correlations may break and Eq. (3) [or (2)] forms the solution.

Master equation results.— The full solution of Eq. (1) can be evaluated efficiently at complexity $\mathcal{O}(N^3)$ by exploiting the statistical equivalence between atoms whose individual decay coefficients γ_F are identical [55–58]. We used PIQS [59] implemented in QuTip [60] where such an algorithm is realized to calculate numerically the density matrix and atomic observables.

In Fig. 2(a), we compare the steady-state population inversion (“magnetization”) $\langle \hat{S}_z \rangle$ from the exact solution of (1) for different atom numbers N , to the mean-field result $Ns_z/2$ with s_z from Eq. (2). For an appropriate comparison, we fix the mean-field parameters Γ

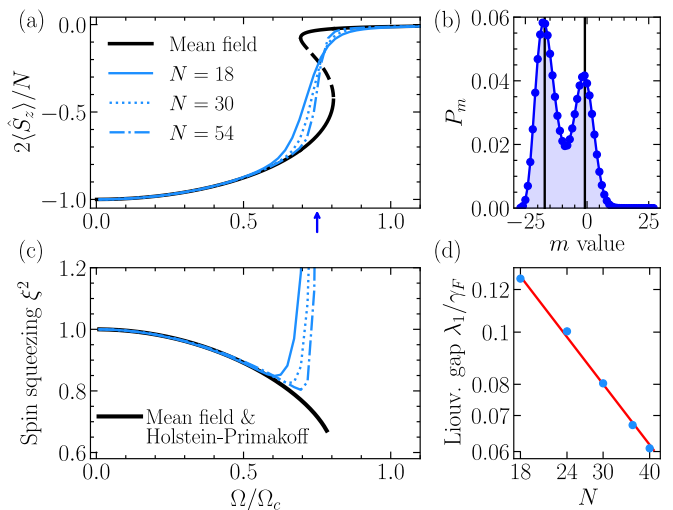


FIG. 2. Numerical solution of the master equation (1) in steady state. The mean-field parameters are fixed to $\Gamma/\gamma = 15.5$ for all values of atom number N (text). (a) Average population inversion (“magnetization”) $\langle \hat{S}_z \rangle$ as a function of the drive Ω (blue curves) compared with the mean-field solution of Eq. (2) (black curve). (b) Probability distribution of the magnetization eigenvalues m exhibits a bimodal form centered at the two stable mean-field solutions (black lines; $N = 54$ and $\Omega = 0.75\Omega_c$). (c) Spin squeezing parameter exhibits quantum correlations $\xi^2 < 1$ up to the bistability region. Black curve displays analytical results from Eq. (7). (d) Liouvillian gap λ_1 (blue dots) fitted as a power-law $1.72N^{-0.9}$ (red curve).

and γ and solve Eq. (1) numerically for each N with $\gamma_{1D} = \Gamma/(N - 1)$ and $\gamma_F = \gamma - \gamma_{1D}$. We observe that while the two solutions agree outside the bistability region predicted by mean-field, the comparison within this region is more subtle since the steady-state ρ_s of Eq. (1) is unique [61]. To capture the bistability effect, we plot in Fig. 2(b) the probability distribution for observing an eigenvalue m of \hat{S}_z , $P_m = \sum_{j=|m|}^{N/2} \langle j, m | \rho_s | j, m \rangle$, with $|j, m\rangle$ being the usual states of angular momentum j . We notice a bimodal distribution centered at two m values, which agree with the stable mean-field solutions.

We also calculate the spin-squeezing parameter $\xi^2 = \min_\varphi \text{Var}[\hat{S}'_\varphi]N / |\langle \hat{S} \rangle|^2$ [62] at steady state ρ_s . Here \hat{S}'_φ is the spin-vector component directed at an angle φ on the plane perpendicular to the mean spin $\langle \hat{S} \rangle$ [with $\hat{S} = (\hat{S}_x, \hat{S}_y, \hat{S}_z)$], and $\xi^2 < 1$ implies spin-squeezing quantum correlations useful in metrology. We observe in Fig. 2(c) that the steady state is squeezed as long as $\langle \hat{S}_z \rangle$ coincides with the lower branch of the mean-field solution [Fig. 2(a)], as discussed further below.

Quantum bistability.— The bimodal distribution in Fig. 2(b) suggests the existence of a first-order phase transition [63]. To explore this possibility in our dissipative quantum system [64], we consider the eigenvalues λ_i and eigenvectors ρ_i of the Liouvillian superoperator \mathcal{L} from Eq. (1). The eigenvalue with the smallest non-vanishing real part is called the Liouvillian gap and de-

noted by λ_1 . Recalling the uniqueness of the steady state $\rho_0 \equiv \rho_s$ ($\lambda_0 = 0$) at finite N , we can write the density matrix at long times $t \gg 1/\lambda_i \forall i \neq 0, 1$ as

$$\rho(t) = \rho_s + c_1 \rho_1 e^{-\lambda_1 t}, \quad (4)$$

with the constant c_1 determined from initial conditions. Following [64] we define a dissipative first-order phase transition by the closing of the Liouvillian gap, $\lambda_1 \rightarrow 0$ for $N \rightarrow \infty$ at some critical drive Ω . In this case, the kernel of the Liouvillian \mathcal{L} becomes two-fold degenerate, leading to two stable phases. We found the Liouvillian gap λ_1 by fitting the long-time dynamics of the magnetization, calculated from Eq. (1), to $\langle \hat{S}_z(t) \rangle - \langle \hat{S}_z(\infty) \rangle \propto e^{-\lambda_1 t}$ [65]. This was performed for different atom numbers N by varying Ω and finding the minimal λ_1 , verifying its agreement with that obtained by a direct diagonalization of \mathcal{L} (the latter being feasible up to $N \leq 24$). The results are plotted in Fig. 2(d), suggesting that the gap indeed closes as $\lambda_1 \propto N^{-0.9}$.

The closing of the gap, $\lambda_1 \rightarrow 0$, implies that ρ_1 tends to enter the kernel and that the steady state encodes two quantum states corresponding to two phases. To determine the two states we decompose ρ_1 , which is seen from Eq. (4) to be traceless, into two physical (trace-1) density matrices, $\rho_1 = \rho_+ - \rho_-$, with ρ_+ (ρ_-) formed by the diagonal matrix containing the positive (negative) eigenvalues of ρ_1 [64]. The latter are orthogonal and approximately span the kernel, allowing to write

$$\rho_s \underset{N \rightarrow \infty}{\simeq} a_+ \rho_+ + a_- \rho_-, \quad a_+ + a_- = 1. \quad (5)$$

Hence, the steady state is given by a statistical mixture of two quantum many-body states. We show this for $N = 18$ by numerically finding ρ_1 as the eigenvector of the smallest nonzero eigenvalue of \mathcal{L} and constructing ρ_{\pm} from its diagonal form. In Fig 3(a), we plot the average of \hat{S}_z taken with ρ_+ and ρ_- , showing their respective agreement with the lower and upper branches of the bistable mean-field solution. The correspondence to the two steady-state phases is further exhibited by the respective distributions of m plotted for $a_{\pm} \rho_{\pm}$ in Fig. 3(b), whose sum recovers the bimodal distribution of ρ_s to a very good approximation. Here $a_+ = 0.4$ and $a_- = 0.5$ were independently obtained from $a_{\pm} = \text{tr}(\rho_s \rho_{\pm}) / \text{tr}[(\rho_{\pm})^2]$ noting their sum tends to 1, as in (5), already for our moderate $N = 18$.

Emergence of Dicke physics.— A deeper understanding of the nature of this bistability is gained by observing that the lower branch of the mean-field solution resembles that of the Dicke problem ($\gamma_F = 0$) [Fig. 3(a)]. Importantly, our quantum analysis then allows to explore the possible emergence of Dicke physics in the full quantum-mechanical sense beyond mean-field, by studying the state ρ_+ associated with the lower branch. To this end, we exploit the fact that the steady state of the Dicke problem is a CRSS, given by an asymptotic eigenstate of \hat{S}_- with eigenvalue $-i2\Omega/\gamma_{1D}$ [22]. Using the CRSS expansion in angular-momentum states $|N/2, m\rangle$ [22], we

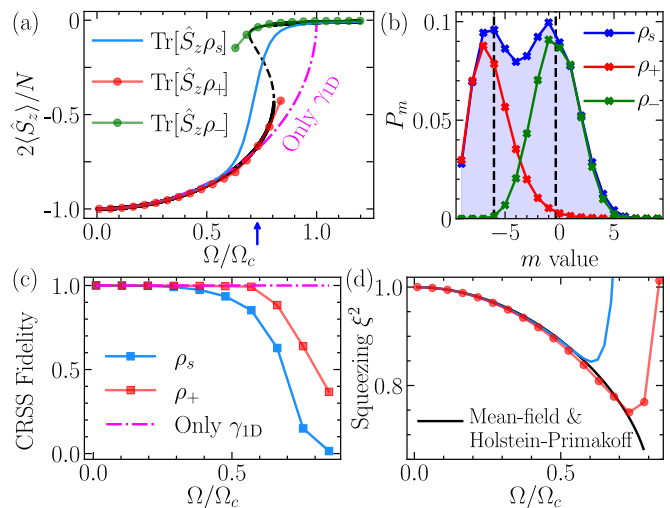


FIG. 3. Steady-state density matrix ρ_s as a mixture of two stable states ρ_{\pm} , Eq. (5). ρ_{\pm} are found numerically for $N = 18$, $\gamma_{1D} = 10\gamma_F$. (a) Average magnetization calculated with ρ_+ (ρ_-) is seen to agree with the lower- (upper-) branch mean-field solution. (b) Magnetization distributions of ρ_{\pm} are centered around the corresponding mean-field values, with their sum (weighted with a_{\pm}) approximately reproducing the bimodal distribution of ρ_s ($\Omega = 0.73\Omega_c$). (c) Fidelity with CRSS. (d) Spin squeezing $\xi^2 < 1$ is exhibited in the CRSS-like state ρ_+ , in agreement with the analytical result, Eq. (7) (black curve).

calculate its overlap with ρ_+ and observe very high fidelities, dropping only towards the end of the bistability region [Fig. 3(c)]. Remarkably, this suggests that all quantum properties of collective CRSS physics should be exhibited by the stable state ρ_+ , including its coherent radiation and spin-squeezing entanglement.

For the latter, more insight can be gained by first evaluating the spin squeezing analytically, adopting a Heisenberg-picture approach [31]. To this end, we begin with the Heisenberg-Langevin equations for $\hat{\sigma}_n$ and $\hat{\sigma}_n^z$ which correspond to Eq. (1). Linearizing the equations for small fluctuations around the lower-branch of the mean-field solution (2) using the Holstein-Primakoff transformation, we find the dynamical equation of collective-spin fluctuations [54],

$$\dot{\hat{a}} = \left(\frac{\Gamma j_{\text{MF}} \cos \theta}{N} - \frac{\gamma}{2} \right) \hat{a} - \frac{\gamma}{4} \sin^2 \theta (\hat{a} - \hat{a}^\dagger) + \sqrt{\frac{j_{\text{MF}}}{2N}} \times \left[\cos \theta (\hat{F} + \hat{F}^\dagger + \hat{\eta} + \hat{\eta}^\dagger) + (\hat{F}^\dagger - \hat{F} + \hat{\eta}^\dagger - \hat{\eta}) \right]. \quad (6)$$

Here $\hat{a} = \frac{1}{\sqrt{N}} \sum_n \hat{a}_n$, $\hat{F} = \sqrt{N} \hat{f}$ and $\hat{\eta} = \frac{1}{\sqrt{N}} \sum_n \hat{\eta}_n$, where \hat{a}_n is the bosonic fluctuation of the spin of atom n , and \hat{f} ($\hat{\eta}_n$) is the vacuum noise associated with collective (individual) decay γ_{1D} (γ_F). The effective spin size $j_{\text{MF}} = |\mathbf{s}|N/2$ and excitation angle $\theta = \arccos(s_z/|\mathbf{s}|)$ with $|\mathbf{s}| = \sqrt{s_x^2 + s_y^2 + s_z^2}$ are given by the lower-branch mean-field solution $s_{x,y,z}$. Within this formulation, the

spin squeezing is obtained as [54]

$$\xi^2 = 1 + 2(\langle \hat{a}^\dagger \hat{a} \rangle - |\langle \hat{a}^2 \rangle|). \quad (7)$$

Solving Eq. (6) for \hat{a} in steady state, and using the correlations of vacuum noises $\langle \hat{f}(t)\hat{f}^\dagger(t') \rangle = \gamma_{1D}\delta(t-t')$, $\langle \hat{\eta}_n(t)\hat{\eta}_m^\dagger(t') \rangle = \gamma_F\delta_{nm}\delta(t-t')$ we obtain an analytical expression for ξ^2 in terms of the mean-field parameters Γ and γ and the lower-branch solution $s_{x,y,z}$. The full analytical expression for ξ^2 is given in [54] and plotted in Fig. 2(c): we observe excellent agreement with the squeezing calculated for the stable state ρ_+ , extending towards the end of the bistability region. In the limiting case $\Gamma \gg \gamma$, substituting the mean-field values from Eq. (3), we get

$$\xi^2 = \frac{1 + \sqrt{1 - 2\Omega^2/\Omega_c^2}}{\sqrt{2}\sqrt{1 + \Omega^2/\Omega_c^2 + \sqrt{1 - 2\Omega^2/\Omega_c^2}}} \xrightarrow{\Omega = \frac{\Omega_c}{\sqrt{2}}} \frac{1}{\sqrt{3}}, \quad (8)$$

yielding the optimal achievable squeezing $1/\sqrt{3}$.

Steady-state dynamics.— The observable physical meaning of the quantum bistability is directly revealed in dynamics. Recalling that the long-time dynamics, Eq. (4), is spanned by ρ_s and ρ_l and hence approximately by ρ_\pm , we use $\rho_l = \rho_+ - \rho_-$ and (5) in Eq. (4), obtaining the density matrix at long-times,

$$\rho(t) = p_+(t)\rho_+ + p_-(t)\rho_-, \quad p_\pm(t) = a_\pm \pm c_1 e^{-\lambda_1 t}. \quad (9)$$

The probabilities $p_\pm(t)$ to find the system in states ρ_\pm then dynamically evolve as

$$\dot{p}_\pm(t) = -\Gamma_\pm p_\pm(t) + \Gamma_\mp p_\mp(t), \quad \Gamma_\pm = \lambda_1 a_\mp. \quad (10)$$

Notably, Eq. (10) describes a two-state Markov process of stochastic jumps between these states at rates Γ_\pm [inset of Fig. 4(a)]. However, unlike a classical Markov process, here, the jumps are activated by quantum-vacuum noise and occur between two states in Liouville space, each of which represents a many-body state with its own quantum statistics and properties. Therefore, we predict a physical reality of dynamical switching not only of an order parameter (here $\langle \hat{S}_z \rangle$), as studied in previous works [66–71], but of the full quantum properties including correlations and entanglement. This prediction is nicely manifest in the simulation of single trajectories from the quantum stochastic unraveling of Eq. (1) [72]: In Fig. 4, we observe the jumps between the two values corresponding to ρ_\pm for: magnetization, fidelity with CRSS, and spin squeezing. The fluctuations around the two values decrease with the system size N [54].

Importantly, the switching rates $\Gamma_\pm \propto \lambda_1$ tend to zero at the critical point as $\lambda_1 \rightarrow 0$ [Fig. 2(d)], implying that the system resides for exceedingly long times in either of the states ρ_+ or ρ_- . For the former, recalling the resemblance of ρ_+ to a CRSS [Figs. 3(c) and 4(b)], this leads to the following remarkable conclusion: namely, that the practically observable physical reality is similar to that

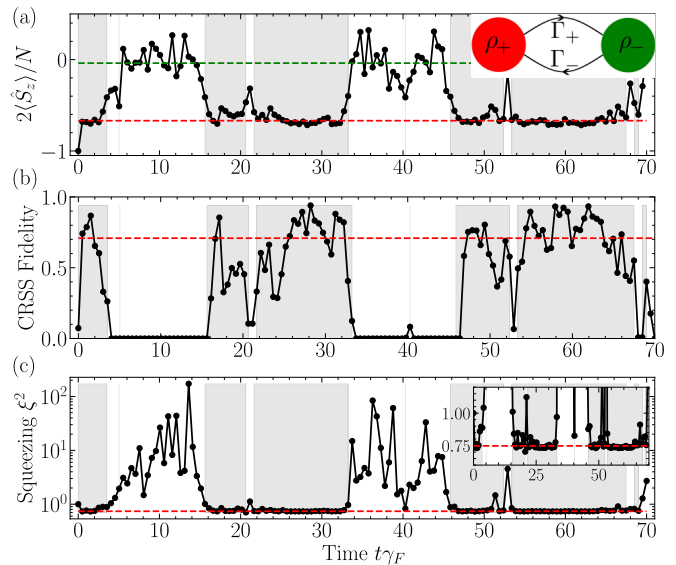


FIG. 4. Quantum switching between stable states ρ_\pm manifest in quantum-trajectory simulations (performed in QuTip [60] for $N = 18$, $\gamma_{1D} = 10\gamma_F$ and $\Omega = 0.73\Omega_c$). (a) Magnetization $\langle \hat{S}_z \rangle$ in a single trajectory is seen to jump between the two mean-field values, also corresponding to ρ_\pm (red and green dashed curves). (b) CRSS fidelity for the same trajectory compared to the CRSS fidelity of ρ_+ (red dashed curve). (c) Spin squeezing on the same trajectory compared to the analytical result from Eq. (7) (red dashed curve). Inset: Same in the region $0.5 < \xi^2 < 1.25$.

of the Dicke problem of purely correlated collective decay, exhibiting metrologically useful spin squeezing and entanglement, even in the presence of decorrelating individual decay. While it might be expected that Dicke physics emerges at short times $t \ll \gamma_F^{-1}$ before individual decay is noticeable [54], here we surprisingly find that this can be the case also at the true steady state for $t \gg \gamma_F^{-1}$.

We stress that Eq. (10), which entails the switching dynamics, was derived by us directly from the theory of dissipative phase transitions, and is used here with our knowledge of ρ_\pm to predict the simulated trajectories of various quantum properties seen in Fig. 4. This is in contrast to previous works where a similar equation was presented as an effective model justified *posteriori* by simulated trajectories of a specific order parameter or its bimodal distribution [67, 69, 73].

Discussion.— We analyzed steady-state collective radiation in the presence of local dissipation. We found a quantum bistability and used CRSS theory to characterize the emergence of correlated Dicke-like physics. These predictions can be readily tested experimentally in common cavity systems by observing the statistics and switching dynamics of atomic properties or radiation. The surprising finding of Dicke-like steady-states beyond the Dicke indistinguishability symmetry entails profound implications on the analysis and interpretation of experiments: considering that any realistic system exhibits local decay at relevant time scales, the observa-

tion of Dicke-like physics then does not necessarily imply negligible local decay, and can result from the CRSS-like quasistable state ρ_+ . More generally, these results establish a first step in a systematic study of the interplay between collective and individual decay. This should be crucial for our understanding and design of prominent quantum platforms and technologies, such as atomic arrays and ensembles [15, 32–34]. Moreover, it opens a new path in the study of dissipative quantum many-body sys-

tems with collective decay.

Acknowledgments.— We acknowledge fruitful discussions with Daniel Goncalves-Romeu and Darrick Chang, and financial support from the Israel Science Foundation (ISF), the ISF and the Directorate for Defense Research and Development (DDR&D), the Center for New Scientists at the Weizmann Institute of Science, the Council for Higher Education (Israel), and QUANTERA (PACE-IN). This research is made possible in part by the historic generosity of the Harold Perlman Family.

-
- [1] M. Gross and S. Haroche, Superradiance: An essay on the theory of collective spontaneous emission, *Physics Reports* **93**, 301 (1982).
- [2] D. Meiser, J. Ye, D. R. Carlson, and M. J. Holland, Prospects for a Millihertz-Linewidth Laser, *Physical Review Letters* **102**, 163601 (2009).
- [3] L. Henriot, J. S. Douglas, D. E. Chang, and A. Albrecht, Critical open-system dynamics in a one-dimensional optical-lattice clock, *Physical Review A* **99**, 023802 (2019).
- [4] D. E. Chang, J. Ye, and M. D. Lukin, Controlling dipole-dipole frequency shifts in a lattice-based optical atomic clock, *Physical Review A* **69**, 023810 (2004), publisher: American Physical Society.
- [5] S. Ostermann, O. Rubies-Bigorda, V. Zhang, and S. F. Yelin, *Breakdown of steady-state superradiance in extended driven atomic arrays* (2023), arXiv:2311.10824 [quant-ph].
- [6] M. A. Norcia, M. N. Winchester, J. R. K. Cline, and J. K. Thompson, Superradiance on the millihertz linewidth strontium clock transition, *Science Advances* **2**, e1601231 (2016), publisher: American Association for the Advancement of Science.
- [7] Y. Kaluzny, P. Goy, M. Gross, J. M. Raimond, and S. Haroche, Observation of Self-Induced Rabi Oscillations in Two-Level Atoms Excited Inside a Resonant Cavity: The Ringing Regime of Superradiance, *Physical Review Letters* **51**, 1175 (1983), publisher: American Physical Society.
- [8] A. Angerer, K. Streltsov, T. Astner, S. Putz, H. Sumiya, S. Onoda, J. Isoya, W. J. Munro, K. Nemoto, J. Schmiedmayer, and J. Majer, Superradiant emission from colour centres in diamond, *Nature Physics* **14**, 1168 (2018), publisher: Nature Publishing Group.
- [9] W. Kersten, N. de Zordo, E. S. Redchenko, N. Lagos, A. N. Kanagin, A. Angerer, W. J. Munro, K. Nemoto, I. E. Mazets, and J. Schmiedmayer, *Self-Induced Superradiant Masing* (2024), arXiv:2402.08537 [quant-ph].
- [10] J. G. Bohnet, Z. Chen, J. M. Weiner, D. Meiser, M. J. Holland, and J. K. Thompson, A steady-state superradiant laser with less than one intracavity photon, *Nature* **484**, 78 (2012), number: 7392 Publisher: Nature Publishing Group.
- [11] G.-D. Lin and S. F. Yelin, Chapter 6 - Superradiance: An Integrated Approach to Cooperative Effects in Various Systems, in *Advances In Atomic, Molecular, and Optical Physics*, Advances in Atomic, Molecular, and Optical Physics, Vol. 61, edited by P. Berman, E. Arimondo, and C. Lin (Academic Press, 2012) pp. 295–329.
- [12] J. Pellegrino, R. Bourgain, S. Jennewein, Y. Sortais, A. Browaeys, S. Jenkins, and J. Ruostekoski, Observation of Suppression of Light Scattering Induced by Dipole-Dipole Interactions in a Cold-Atom Ensemble, *Physical Review Letters* **113**, 133602 (2014).
- [13] W. Kersten, N. de Zordo, O. Diekmann, T. Reiter, M. Zens, A. N. Kanagin, S. Rotter, J. Schmiedmayer, and A. Angerer, Triggered Superradiance and Spin Inversion Storage in a Hybrid Quantum System, *Physical Review Letters* **131**, 043601 (2023), publisher: American Physical Society.
- [14] D. D. Grimes, S. L. Coy, T. J. Barnum, Y. Zhou, S. F. Yelin, and R. W. Field, Direct single-shot observation of millimeter-wave superradiance in Rydberg-Rydberg transitions, *Physical Review A* **95**, 043818 (2017), publisher: American Physical Society.
- [15] G. Ferioli, A. Glicenstein, I. Ferrier-Barbut, and A. Browaeys, A non-equilibrium superradiant phase transition in free space, *Nature Physics* **19**, 1345 (2023), number: 9 Publisher: Nature Publishing Group.
- [16] S. J. Masson and A. Asenjo-Garcia, Universality of Dicke superradiance in arrays of quantum emitters, *Nature Communications* **13**, 2285 (2022), number: 1 Publisher: Nature Publishing Group.
- [17] A. Ishizaki and G. R. Fleming, Quantum Coherence in Photosynthetic Light Harvesting, *Annual Review of Condensed Matter Physics* **3**, 333 (2012), publisher: Annual Reviews.
- [18] A. González-Tudela, V. Paulisch, D. Chang, H. Kimble, and J. Cirac, Deterministic Generation of Arbitrary Photonic States Assisted by Dissipation, *Physical Review Letters* **115**, 163603 (2015), publisher: American Physical Society.
- [19] Z. Wang, T. Jaako, P. Kirton, and P. Rabl, Supercorrelated Radiance in Nonlinear Photonic Waveguides, *Physical Review Letters* **124**, 213601 (2020), publisher: American Physical Society.
- [20] C. Hotter, L. Ostermann, and H. Ritsch, Cavity sub- and superradiance for transversely driven atomic ensembles, *Physical Review Research* **5**, 013056 (2023), publisher: American Physical Society.
- [21] R. H. Dicke, Coherence in Spontaneous Radiation Processes, *Physical Review* **93**, 99 (1954).
- [22] O. Somech and E. Shahmoon, Quantum Entangled States of a Classically Radiating Macroscopic Spin, *PRX Quantum* **5**, 010349 (2024), publisher: American Physical Society.
- [23] P. D. Drummond and H. J. Carmichael, Volterra cycles and the cooperative fluorescence critical point, *Optics*

- Communications* **27**, 160 (1978).
- [24] H. J. Carmichael, Analytical and numerical results for the steady state in cooperative resonance fluorescence, *Journal of Physics B: Atomic and Molecular Physics* **13**, 3551 (1980).
- [25] E. M. Kessler, G. Giedke, A. Imamoglu, S. F. Yelin, M. D. Lukin, and J. I. Cirac, Dissipative phase transition in a central spin system, *Physical Review A* **86**, 012116 (2012).
- [26] C. Sánchez Muñoz, B. Buča, J. Tindall, A. González-Tudela, D. Jaksch, and D. Porras, Symmetries and conservation laws in quantum trajectories: Dissipative freezing, *Physical Review A* **100**, 042113 (2019), publisher: American Physical Society.
- [27] D. Barberena, R. J. Lewis-Swan, J. K. Thompson, and A. M. Rey, Driven-dissipative quantum dynamics in ultra-long-lived dipoles in an optical cavity, *Physical Review A* **99**, 053411 (2019), publisher: American Physical Society.
- [28] A. Gonzalez-Tudela and D. Porras, Mesoscopic Entanglement Induced by Spontaneous Emission in Solid-State Quantum Optics, *Physical Review Letters* **110**, 080502 (2013), arXiv:1209.4730 [cond-mat, physics:quant-ph].
- [29] T. E. Lee, C.-K. Chan, and S. F. Yelin, Dissipative phase transitions: Independent versus collective decay and spin squeezing, *Physical Review A* **90**, 052109 (2014).
- [30] C. Qu and A. M. Rey, Spin squeezing and many-body dipolar dynamics in optical lattice clocks, *Physical Review A* **100**, 041602 (2019), publisher: American Physical Society.
- [31] O. Somech, Y. Shimshi, and E. Shahmoon, Heisenberg-Langevin approach to driven superradiance, *Physical Review A* **108**, 023725 (2023), publisher: American Physical Society.
- [32] I. Bloch, Ultracold quantum gases in optical lattices, *Nature Physics* **1**, 23 (2005), publisher: Nature Publishing Group.
- [33] D. Barredo, S. de Léséleuc, V. Lienhard, T. Lahaye, and A. Browaeys, An atom-by-atom assembler of defect-free arbitrary two-dimensional atomic arrays, *Science* **354**, 1021 (2016), publisher: American Association for the Advancement of Science.
- [34] M. Endres, H. Bernien, A. Keesling, H. Levine, E. R. Anschuetz, A. Krajenbrink, C. Senko, V. Vuletic, M. Greiner, and M. D. Lukin, Atom-by-atom assembly of defect-free one-dimensional cold atom arrays, *Science* **354**, 1024 (2016).
- [35] J. Rui, D. Wei, A. Rubio-Abadal, S. Hollerith, J. Zeiher, D. M. Stamper-Kurn, C. Gross, and I. Bloch, A subradiant optical mirror formed by a single structured atomic layer, *Nature* **583**, 369 (2020), number: 7816 Publisher: Nature Publishing Group.
- [36] R. J. Bettles, S. A. Gardiner, and C. S. Adams, Enhanced Optical Cross Section via Collective Coupling of Atomic Dipoles in a 2D Array, *Physical Review Letters* **116**, 103602 (2016), publisher: American Physical Society.
- [37] E. Shahmoon, D. S. Wild, M. D. Lukin, and S. F. Yelin, Cooperative Resonances in Light Scattering from Two-Dimensional Atomic Arrays, *Physical Review Letters* **118**, 113601 (2017), publisher: American Physical Society.
- [38] A. Asenjo-Garcia, M. Moreno-Cardoner, A. Albrecht, H. Kimble, and D. Chang, Exponential Improvement in Photon Storage Fidelities Using Subradiance and “Selective Radiance” in Atomic Arrays, *Physical Review X* **7**, 031024 (2017), publisher: American Physical Society.
- [39] A. Grankin, P. O. Guimond, D. V. Vasilyev, B. Vermaersch, and P. Zoller, Free-space photonic quantum link and chiral quantum optics, *Physical Review A* **98**, 043825 (2018), publisher: American Physical Society.
- [40] A. Cidrim, T. Do Espirito Santo, J. Schachenmayer, R. Kaiser, and R. Bachelard, Photon Blockade with Ground-State Neutral Atoms, *Physical Review Letters* **125**, 073601 (2020).
- [41] C. D. Parmee and J. Ruostekoski, Bistable optical transmission through arrays of atoms in free space, *Physical Review A* **103**, 033706 (2021), publisher: American Physical Society.
- [42] F. Robicheaux and D. A. Suresh, Beyond lowest order mean-field theory for light interacting with atom arrays, *Physical Review A* **104**, 023702 (2021), publisher: American Physical Society.
- [43] D. Fernández-Fernández and A. González-Tudela, Tunable Directional Emission and Collective Dissipation with Quantum Metasurfaces, *Physical Review Letters* **128**, 113601 (2022), publisher: American Physical Society.
- [44] S. P. Pedersen, L. Zhang, and T. Pohl, Quantum nonlinear metasurfaces from dual arrays of ultracold atoms, *Physical Review Research* **5**, L012047 (2023), publisher: American Physical Society.
- [45] Y. Solomons, R. Ben-Maimon, and E. Shahmoon, *Universal approach for quantum interfaces with atomic arrays* (2023), arXiv:2302.04913 [quant-ph].
- [46] Z. Yan, J. Ho, Y.-H. Lu, S. J. Masson, A. Asenjo-Garcia, and D. M. Stamper-Kurn, Superradiant and Subradiant Cavity Scattering by Atom Arrays, *Physical Review Letters* **131**, 253603 (2023), publisher: American Physical Society.
- [47] K. Hammerer, A. S. Sørensen, and E. S. Polzik, Quantum interface between light and atomic ensembles, *Reviews of Modern Physics* **82**, 1041 (2010).
- [48] S. L. Bromley, B. Zhu, M. Bishof, X. Zhang, T. Bothwell, J. Schachenmayer, T. L. Nicholson, R. Kaiser, S. F. Yelin, M. D. Lukin, A. M. Rey, and J. Ye, Collective atomic scattering and motional effects in a dense coherent medium, *Nature Communications* **7**, 11039 (2016), number: 1 Publisher: Nature Publishing Group.
- [49] W. Guerin, M. O. Araújo, and R. Kaiser, Subradiance in a Large Cloud of Cold Atoms, *Physical Review Letters* **116**, 083601 (2016), publisher: American Physical Society.
- [50] B. Olmos, D. Yu, and I. Lesanovsky, Steady-state properties of a driven atomic ensemble with nonlocal dissipation, *Physical Review A* **89**, 023616 (2014).
- [51] D. Goncalves, L. Bombieri, G. Ferioli, S. Pancaldi, I. Ferrier-Barbut, A. Browaeys, E. Shahmoon, and D. E. Chang, *Driven-dissipative phase separation in free-space atomic ensembles* (2024), arXiv:2403.15237 [quant-ph].
- [52] S. Agarwal, E. Chaparro, D. Barberena, A. P. Orioli, G. Ferioli, S. Pancaldi, I. Ferrier-Barbut, A. Browaeys, and A. M. Rey, *Directional superradiance in a driven ultracold atomic gas in free-space* (2024), arXiv:2403.15556 [cond-mat, physics:physics, physics:quant-ph].
- [53] K. Tucker, D. Barberena, R. J. Lewis-Swan, J. K. Thompson, J. G. Restrepo, and A. M. Rey, Facilitating spin squeezing generated by collective dynamics with single-particle decoherence, *Physical Review A* **102**,

- 051701 (2020).
- [54] See Supplementary Information for details of derivation which includes Refs. [74, 75].
- [55] M. Xu, D. A. Tieri, and M. J. Holland, Simulating open quantum systems by applying SU(4) to quantum master equations, *Physical Review A* **87**, 062101 (2013).
- [56] F. Damanet, D. Braun, and J. Martin, Cooperative spontaneous emission from indistinguishable atoms in arbitrary motional quantum states, *Physical Review A* **94**, 033838 (2016).
- [57] N. Shammah, N. Lambert, F. Nori, and S. De Liberato, Superradiance with local phase-breaking effects, *Physical Review A* **96**, 023863 (2017), publisher: American Physical Society.
- [58] Y. Zhang, Y.-X. Zhang, and K. Mølmer, Monte-Carlo simulations of superradiant lasing, *New Journal of Physics* **20**, 112001 (2018), publisher: IOP Publishing.
- [59] N. Shammah, S. Ahmed, N. Lambert, S. De Liberato, and F. Nori, Open quantum systems with local and collective incoherent processes: Efficient numerical simulations using permutational invariance, *Physical Review A* **98**, 063815 (2018), publisher: American Physical Society.
- [60] J. R. Johansson, P. D. Nation, and F. Nori, QuTiP 2: A Python framework for the dynamics of open quantum systems, *Computer Physics Communications* **184**, 1234 (2013).
- [61] D. Nigro, On the uniqueness of the steady-state solution of the Lindblad–Gorini–Kossakowski–Sudarshan equation, *Journal of Statistical Mechanics: Theory and Experiment* **2019**, 043202 (2019).
- [62] J. Ma, X. Wang, C. P. Sun, and F. Nori, Quantum spin squeezing, *Physics Reports* **509**, 89 (2011).
- [63] K. Binder and D. P. Landau, Finite-size scaling at first-order phase transitions, *Physical Review B* **30**, 1477 (1984), publisher: American Physical Society.
- [64] F. Minganti, A. Biella, N. Bartolo, and C. Ciuti, Spectral theory of Liouvillians for dissipative phase transitions, *Physical Review A* **98**, 042118 (2018), publisher: American Physical Society.
- [65] F. Vicentini, F. Minganti, R. Rota, G. Orso, and C. Ciuti, Critical slowing down in driven-dissipative Bose-Hubbard lattices, *Physical Review A* **97**, 013853 (2018), publisher: American Physical Society.
- [66] T. E. Lee, H. Häffner, and M. C. Cross, Collective Quantum Jumps of Rydberg Atoms, *Physical Review Letters* **108**, 023602 (2012), publisher: American Physical Society.
- [67] R. M. Wilson, K. W. Mahmud, A. Hu, A. V. Gorshkov, M. Hafezi, and M. Foss-Feig, Collective phases of strongly interacting cavity photons, *Physical Review A* **94**, 033801 (2016), publisher: American Physical Society.
- [68] J. Gelhausen and M. Buchhold, Dissipative Dicke model with collective atomic decay: Bistability, noise-driven activation, and the nonthermal first-order superradiance transition, *Physical Review A* **97**, 023807 (2018), publisher: American Physical Society.
- [69] P. Brookes, G. Tancredi, A. D. Patterson, J. Rahamim, M. Esposito, T. K. Mavrogordatos, P. J. Leek, E. Ginossar, and M. H. Szymanska, Critical slowing down in circuit quantum electrodynamics, *Science Advances* **7**, eabe9492 (2021), publisher: American Association for the Advancement of Science.
- [70] F. Minganti, V. Savona, and A. Biella, Dissipative phase transitions in n -photon driven quantum nonlinear resonators, *Quantum* **7**, 1170 (2023), arXiv:2303.03355 [quant-ph].
- [71] B. Gábor, D. Nagy, A. Vukics, and P. Domokos, Quantum bistability in the hyperfine ground state of atoms, *Physical Review Research* **5**, L042038 (2023), publisher: American Physical Society.
- [72] K. Mølmer, Y. Castin, and J. Dalibard, Monte Carlo wave-function method in quantum optics, *JOSA B* **10**, 524 (1993), publisher: Optica Publishing Group.
- [73] C. Savage and H. Carmichael, Single atom optical bistability, *IEEE Journal of Quantum Electronics* **24**, 1495 (1988), conference Name: IEEE Journal of Quantum Electronics.
- [74] Y. Solomons and E. Shahmoon, Multichannel waveguide QED with atomic arrays in free space, *Physical Review A* **107**, 033709 (2023), publisher: American Physical Society.
- [75] M. W. Hirsch, R. L. Devaney, and S. Smale, *Differential Equations, Dynamical Systems, and Linear Algebra* (Elsevier Science & Technology, San Diego, United States, 1974).

Supplemental Material for “Quantum bistability at the interplay between collective and individual decay”

S1. DERIVATION OF BASIC EQUATIONS OF MOTION

A. System and Hamiltonian

We consider N two-level atoms inside a driven one-sided optical cavity. We assume that atoms are identically coupled to the cavity mode (e.g. located at cavity antinodes). The Hamiltonian for the atoms and the cavity mode is given by

$$\mathcal{H}_S = \hbar\omega_0 \sum_n \hat{\sigma}_n^\dagger \hat{\sigma}_n + \hbar\omega_c \hat{c}^\dagger \hat{c} + \hbar \sum_n (g^* \hat{c}^\dagger \hat{\sigma}_n + g \hat{\sigma}_n^\dagger \hat{c}) + \hbar(\Omega_L \hat{c}^\dagger e^{-i\omega_L t} + \Omega_L^* \hat{c} e^{i\omega_L t}), \quad (\text{S1})$$

where $\hat{\sigma}_n$ is the Pauli lowering operator for atom n with resonant frequency ω_0 , \hat{c} is the boson lowering operator for the cavity mode of frequency ω_c and g is a dipole coupling strength identical for all atoms. The external laser comes from the left side of the cavity with amplitude Ω_L and frequency ω_L .

The cavity mode is coupled through the left mirror to the 1D continuum of the propagating photon modes with the wave numbers k and frequencies $\omega_k = c|k|$ (c being the speed of light)

$$\mathcal{H}_R = \hbar \sum_{k<0} \omega_k \hat{b}_k^\dagger \hat{b}_k, \quad \mathcal{H}_{SR} = \hbar \sum_{k<0} (g_c \hat{b}_k^\dagger \hat{c} + g_c^* \hat{c}^\dagger \hat{b}_k), \quad (\text{S2})$$

where \hat{b}_k are the corresponding boson lowering operators and g_c the coupling strength.

Emission to off-axis modes outside the cavity is accounted for by approximating these modes as free-space modes described by the lowering operators $\hat{a}_{\mathbf{k},\mu}$ and frequencies $\omega_{\mathbf{k}} = c|\mathbf{k}|$, with \mathbf{k} the wavevector and μ the polarization:

$$\mathcal{H}_F = \hbar \sum_{\mathbf{k},\mu} \omega_{\mathbf{k}} \hat{a}_{\mathbf{k},\mu}^\dagger \hat{a}_{\mathbf{k},\mu}, \quad \mathcal{H}_{SF} = \hbar \sum_{\mathbf{k},\mu} \sum_n \left(g_{\mathbf{k},\mu,n}^* \hat{a}_{\mathbf{k},\mu}^\dagger \hat{\sigma}_n + g_{\mathbf{k},\mu,n} \hat{\sigma}_n^\dagger \hat{a}_{\mathbf{k},\mu} \right), \quad (\text{S3})$$

where $g_{\mathbf{k},\mu,n} \propto e^{i\mathbf{k}\cdot\mathbf{r}_n}$ is the dipole coupling whose dependence on the atomic position \mathbf{r}_n follows from the free-space plane waves \mathbf{k} .

B. Derivation of the Heisenberg-Langevin equations

In this section, we eliminate the reservoir modes to obtain the equations on the atomic variables. We begin with the equation for the cavity mode, obtained by solving the Heisenberg equation for the 1D continuum modes \hat{b}_k ,

$$\dot{\hat{b}}_k = -i\omega_k \hat{b}_k - ig_c \hat{c} \Rightarrow \hat{b}_k(t) = \hat{b}_k(0) e^{-i\omega_k t} - ig_c \int_0^t dt' \hat{c}(t') e^{i\omega_k(t-t')}, \quad (\text{S4})$$

and insert the solution into the Heisenberg equation for the cavity mode $\hat{c}(t)$. Then, switching to the laser-rotating frame $\tilde{c}(t) = \hat{c}(t) e^{i\omega_L t}$, $\tilde{\sigma}_n(t) = \hat{\sigma}_n(t) e^{i\omega_L t}$ and treating the 1D continuum as a reservoir, we take a Born-Markov type approximation and obtain the Heisenberg-Langevin equation for $\tilde{c}(t)$,

$$\dot{\tilde{c}}(t) = i\delta_c \tilde{c}(t) - \frac{\varkappa}{2} \tilde{c}(t) - ig \sum_n \tilde{\sigma}_n + \hat{E}(t) - i\Omega_L. \quad (\text{S5})$$

Here we introduced the laser detuning from the cavity $\delta_c = \omega_L - \omega_c$ and vacuum noise of the reservoir $\hat{E}(t) = -ig_c^* \sum_k \hat{b}_k(0) e^{-i(\omega_k - \omega_L)t}$, $\langle \hat{E}(t) \rangle = 0$, with the time correlator

$$\langle \hat{E}(t) \hat{E}^\dagger(t') \rangle = |g_c|^2 \sum_{k,k'} \langle \hat{b}_k(0) \hat{b}_{k'}^\dagger(0) \rangle e^{-i\omega_k t + i\omega_{k'} t'} = \varkappa \delta(t - t'), \quad (\text{S6})$$

where $\varkappa = 2|g_c|^2 L/c$ and L is the quantization length of the 1D continuum. We work in the fast cavity limit, assuming \varkappa is much faster than the timescale of variations in $\tilde{\sigma}_n$. This allows us to adiabatically eliminate the cavity mode, which can be effectively achieved by solving Eq. (S5) in the steady state

$$\tilde{c}(t) = \frac{i\Omega_L + ig \sum_n \tilde{\sigma}_n(t) - \hat{E}(t)}{i\delta - \varkappa/2}, \quad (\text{S7})$$

and insert this solution, together with that for the free-space modes $\hat{a}_{\mathbf{k}}$

$$\dot{\hat{a}}_{\mathbf{k},\mu}(t) = -i\omega \hat{a}_{\mathbf{k},\mu}(t) - i \sum_n g_{\mathbf{k},\mu,n}^* \tilde{\sigma}_n(t) \Rightarrow \hat{a}_{\mathbf{k},\mu}(t) = \hat{a}_{\mathbf{k},\mu}(0) e^{-i\omega_{\mathbf{k}} t} - i \sum_n g_{\mathbf{k},\mu,n}^* \int dt' \tilde{\sigma}_n(t') e^{i\omega_{\mathbf{k}}(t-t')}, \quad (\text{S8})$$

into the Heisenberg equation of motion of the Pauli lowering operator of an atom n

$$\dot{\tilde{\sigma}}_n = i\delta \tilde{\sigma}_n + i\Omega \hat{\sigma}_n^z(t) + i\Delta \hat{\sigma}_n^z(t) \sum_m \tilde{\sigma}_m(t) + \frac{\gamma_{1D}}{2} \hat{\sigma}_n^z(t) \sum_m \tilde{\sigma}_m(t) + \hat{\sigma}_n^z(t) \sum_m D(\mathbf{r}_n - \mathbf{r}_m) \tilde{\sigma}_m(t) + [\hat{f}(t) + \hat{\eta}_n(t)] \hat{\sigma}_n^z(t). \quad (\text{S9})$$

Here we introduced the effective drive Rabi frequency Ω , atom-laser detuning δ , emission rate via the cavity mode γ_{1D} and collective shift Δ that describes the resonant dipole-dipole interaction between pairs of atoms

$$\Omega = \frac{ig\Omega_L}{i\delta_c - \varkappa/2}, \quad \delta = \omega_L - \omega_0, \quad \gamma_{1D} = \frac{2g^2 \varkappa}{2\delta_c^2 + \varkappa^2/2}, \quad \Delta = \frac{\delta_c g^2}{\delta_c^2 + \varkappa^2/4}. \quad (\text{S10})$$

The vacuum noise $\hat{f}(t)$ in Eq. (S9) is a vacuum noise of the 1D modes reservoir $\hat{E}(t)$ filtered by the cavity:

$$\hat{f}(t) = -\frac{ig}{i\delta_c - \varkappa/2} \hat{E}(t), \quad \langle \hat{f}(t) \rangle = 0, \quad \langle \hat{f}(t) \hat{f}^\dagger(t') \rangle = \frac{g^2}{\delta_c^2 + \varkappa^2/4} \langle \hat{E}(t) \hat{E}^\dagger(t') \rangle = \gamma_{1D} \delta(t-t'). \quad (\text{S11})$$

The assumed fast cavity regime is realized when the cavity decay rate is much faster than the atom emission rate through the cavity $\gamma_{1D} \ll \varkappa \Rightarrow 4g^2 \ll \varkappa^2$ at $\delta_c = 0$.

The elimination of the free-space modes $\hat{a}_{\mathbf{k},\mu}$ was also performed here within a Born-Markov type approximation, yielding the dipole-dipole interaction $D(\mathbf{r}_n - \mathbf{r}_m)$ mediated by the free-space field modes between different atoms, proportional to the photon Green's function [74]. For inter-atomic distances exceeding the optical wavelength, $|\mathbf{r}_n - \mathbf{r}_m| \gg \lambda = 2\pi c/\omega_L$, this coupling becomes negligible, and we approximate $D(\mathbf{r}_n - \mathbf{r}_m) \approx \delta_{nm} \gamma_F/2$, yielding an individual-atom decay at the rate γ_F of spontaneous emission to free-space. The dissipation induced by the reservoir of modes $\hat{a}_{\mathbf{k},\mu}$ is accompanied by the vacuum-field Langevin noise

$$\hat{\eta}_n(t) = i \sum_{\mathbf{k},\mu} g_{\mathbf{k},\mu,n} \hat{a}_{\mathbf{k},\mu}(0) e^{-i(\omega_{\mathbf{k}} - \omega_L)t}, \quad \langle \hat{\eta}_n(t) \rangle = 0, \quad \langle \hat{\eta}_n(t) \hat{\eta}_m^\dagger(t') \rangle \approx \gamma_F \delta_{nm} \delta(t-t'). \quad (\text{S12})$$

Finally, taking resonant conditions $\delta = \delta_c = 0$, we obtain the Heisenberg-Langevin equation

$$\dot{\tilde{\sigma}}_n(t) = -\frac{\gamma_F}{2} \tilde{\sigma}_n(t) + i\Omega \hat{\sigma}_n^z(t) + \frac{\gamma_{1D}}{2} \hat{\sigma}_n^z(t) \sum_m \tilde{\sigma}_m(t) + \hat{\sigma}_n^z(t) [\hat{f}(t) + \hat{\eta}_n(t)]. \quad (\text{S13})$$

A similar procedure leads to the Heisenberg equation for $\hat{\sigma}_n^z$, obtaining

$$\dot{\hat{\sigma}}_n^z(t) = -\gamma_F (1 + \hat{\sigma}_n^z(t)) - 2 \left[\hat{\sigma}_n^\dagger(t) \left(\hat{f}(t) + \hat{\eta}_n(t) + i\Omega + \frac{\gamma_{1D}}{2} \sum_m \tilde{\sigma}_m(t) \right) + \text{H.c.} \right]. \quad (\text{S14})$$

C. Equivalent master equation

The Heisenberg-Langevin equations (S13) and (S14) are equivalent to the density matrix equation [also Eq. (1) in the main text]

$$\dot{\rho} = -\mathcal{L}[\rho] = -2i\Omega [\hat{S}_x, \rho] + \frac{\gamma_{1D}}{2} \left(2\hat{S}_- \rho \hat{S}_+ - \rho \hat{S}_+ \hat{S}_- - \hat{S}_+ \hat{S}_- \rho \right) + \frac{\gamma_F}{2} \sum_{n=1}^N (2\hat{\sigma}_n \rho \hat{\sigma}_n^\dagger - \rho \hat{\sigma}_n^\dagger \hat{\sigma}_n - \hat{\sigma}_n^\dagger \hat{\sigma}_n \rho). \quad (\text{S15})$$

It could be rewritten as

$$\dot{\rho} = -i(\mathcal{H}_{\text{eff}}\rho(t) - \rho(t)\mathcal{H}_{\text{eff}}) + \sum_{i=1}^{N+1} \mathcal{C}_i\rho(t)\mathcal{C}_i^\dagger, \quad (\text{S16})$$

where we introduce the non-Hermitian Hamiltonian $\mathcal{H}_{\text{eff}} = 2\Omega\hat{S}_x - \frac{i}{2}\sum_{i=1}^{N+1}\mathcal{C}_i^\dagger\mathcal{C}_i$ and jump operators $\mathcal{C} = \{\sqrt{\gamma_{\text{1D}}}\hat{S}_-, \sqrt{\gamma_F}\hat{\sigma}_1, \dots, \sqrt{\gamma_F}\hat{\sigma}_N\}$. Such form is used in Quantum Monte-Carlo trajectories simulations shown in Fig. 4 of the main text.

S2. MEAN-FIELD SOLUTION

A. Derivation of the mean-field equations

The mean-field equation could be obtained either from tracing the master equation (S15) with the required operator and performing averaging, or directly averaging the Heisenberg-Langevin Eqs. (S13) and (S14). We define the mean-field values assuming that they are equal for different atoms $\langle\hat{\sigma}_n\rangle = s_n = s$ and $\langle\hat{\sigma}_n^z\rangle = s_n^z = s_z$ (with the simplified notation $\hat{\sigma}_n \rightarrow \hat{\sigma}_n$ from here on). To deal with the multiplications of the operators that exist in Eqs. (S13)-(S14), we use individual atom factorization

$$\langle\hat{\sigma}_n^\dagger\hat{\sigma}_m\rangle = s^*s = |s|^2 \quad n \neq m, \quad (\text{S17})$$

that is appropriate when the total momentum $\hat{\mathbf{S}}^2 = \hat{S}_x^2 + \hat{S}_y^2 + \hat{S}_z^2$ is not conserved, as in the case of additional individual decay [23].

Following this procedure, we obtain the system of mean-field nonlinear differential equations

$$\begin{cases} \dot{s}_x = -\frac{\gamma}{2}s_x + \frac{\Gamma}{2}s_zs_x, \\ \dot{s}_y = -\frac{\gamma}{2}s_y - 2\Omega s_z + \frac{\Gamma}{2}s_zs_y, \\ \dot{s}_z = -\gamma(s_z + 1) + 2\Omega s_y - \frac{\Gamma}{2}(s_x^2 + s_y^2), \end{cases} \quad (\text{S18})$$

where we defined x, y components as $s_x = s + s^*$, $s_y = i(s - s^*)$ and took the effective Rabi drive frequency Ω to be real without loss of generality. The obtained effective mean-field parameters are related to the model parameters γ_{1D} , γ_F and N from Eq. (S15) by

$$\gamma = \gamma_F + \gamma_{\text{1D}}, \quad \Gamma = (N - 1)\gamma_{\text{1D}}. \quad (\text{S19})$$

From the system of equations (S18) one can see that the total spin $\langle\hat{\mathbf{S}}^2\rangle_{\text{MF}} = N^2(s_x^2 + s_y^2 + s_z^2)/4$ is indeed not conserved

$$\frac{d\langle\hat{\mathbf{S}}^2\rangle_{\text{MF}}}{dt} = -\frac{\gamma N^2}{2}\left(s_z^2 + s_z + \frac{s_x^2 + s_y^2}{2}\right), \quad (\text{S20})$$

and, therefore, utilization of the individual atom factorization is consistent.

In the main text, we compare the results of the mean-field and the master equation (S15) with the Dicke $\hat{\mathbf{S}}^2$ -conserved model with $\gamma_F = 0$ extensively studied before [22, 23]. In this case, the mean-field solution that is verified by the exact master equation solution [22] is obtained using collective products factorization [23]

$$\langle\hat{S}\hat{S}_z\rangle = \langle\hat{S}\rangle\langle\hat{S}_z\rangle.$$

Such factorization will lead to the same equations (S18) with the relation to the master equation parameters $\gamma = 0$ and $\Gamma \rightarrow \Gamma_c = N\gamma_{\text{1D}}$. That factorization is consistent with $\hat{\mathbf{S}}^2$ -invariance and gives unique physical steady state [31]

$$s_x = 0, \quad s_y = \frac{\Omega}{\Omega_c}, \quad s_z = -\sqrt{1 - \frac{\Omega^2}{\Omega_c^2}} \quad (\text{S21})$$

for $\Omega \leq \Omega_c$ where $\Omega_c = \Gamma_c/4$ is a critical value for this model. In the main text, to compare the two models, we use Eq. (S21) with $\Gamma_c = \Gamma$ given by (S19) assuming that the number of atoms is large.

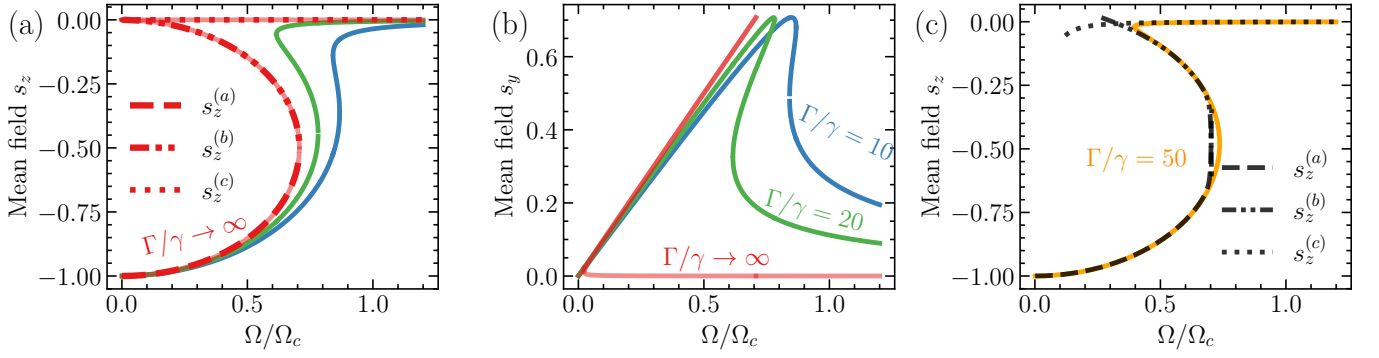


FIG. S1. (a) Numerical solution of Eq. (S22) (solid curves) for $\Gamma/\gamma = 10, 20, 1000$ (blue, green, light red curves). The latter nicely fits the asymptotic analytical result from the three branches of the solution in Eq. (S27) (red dashed, red dotted, and red dashed-dotted curves). (b) Mean-field value of s_y obtained from numerical solution for s_z and Eq. (S23). (c) Numerical solution of Eq. (S22) (orange curve) compared with analytical perturbation expansion up to $\mathcal{O}(\gamma^3)$ (black curves) for $\Gamma/\gamma = 50$.

B. Steady-state solution

The steady-state solution, obtained after setting all the time derivatives in Eq. (S18), reduces to the following cubic equation on s_z :

$$\gamma((1 + s_z)(\gamma - s_z\Gamma)^2 + 8s_z\Omega^2) = 0, \quad (\text{S22})$$

with $s_x = 0$ and s_y expressed through s_z as

$$s_y = -\frac{4s_z\Omega}{\gamma - s_z\Gamma}. \quad (\text{S23})$$

Calculating the discriminant of Eq. (S22) we find that depending on the drive Rabi frequency Ω this polynomial has three real solutions in the region

$$\frac{1}{2}\sqrt{1 + \frac{20\gamma}{\Gamma} - \frac{8\gamma^2}{\Gamma^2} - \sqrt{\left(1 - \frac{8\gamma}{\Gamma}\right)^3}} < \frac{\Omega}{\Omega_c} < \frac{1}{2}\sqrt{1 + \frac{20\gamma}{\Gamma} - \frac{8\gamma^2}{\Gamma^2} + \sqrt{\left(1 - \frac{8\gamma}{\Gamma}\right)^3}}. \quad (\text{S24})$$

We could obtain approximate analytical solutions for s_z from (S22) using perturbation theory. We write the perturbative solution of s_z in the small parameter γ/Γ

$$s_z = s_z^{(0)} + s_z^{(1)}\gamma + s_z^{(2)}\gamma^2 + \mathcal{O}(\gamma^3) \quad (\text{S25})$$

and then substitute it into Eq. (S22) equating the coefficients between γ . In the zeroth order, we have

$$8s_z^{(0)}\Omega^2 + 16(s_z^{(0)})^2 + 16(s_z^{(0)})^3\Omega_c^2 = 0. \quad (\text{S26})$$

Since the equation is cubic, we will have three solutions that we denote as (a), (b), and (c):

$$s_z^{(0,a)} = -\frac{1}{2} \mp \frac{1}{2}\sqrt{1 - \frac{2\Omega^2}{\Omega_c^2}}, \quad s_z^{(0,c)} = 0. \quad (\text{S27})$$

We compare Eq. (S27) with the numerical solution of Eq. (S22) in Fig. S1(a) and see that it perfectly fits for large enough Γ/γ . In terms of the master equation parameters Eq. (S19), the condition $\Gamma \gg \gamma$ is achieved if $N \gg 1$.

Notably, the result (S27) is in stark contrast to that of Eq. (S21), even though it can correspond to taking $\gamma_F/\gamma_{1D} \rightarrow 0$ and $N \rightarrow \infty$ in the mean-field equation (S22). This originated in the decorrelated mean-field assumption taken to arrive to Eq. (S22), which should hold for any finite $\gamma_F > 0$ as long as we wait sufficiently long time $t \gg \gamma_F^{-1}$ to reach the "true" steady state. In contrast, the Dicke regime, Eq. (S21), is then expected to be a good approximation for $t \ll \gamma_F^{-1}$, see Sec. S4 below.

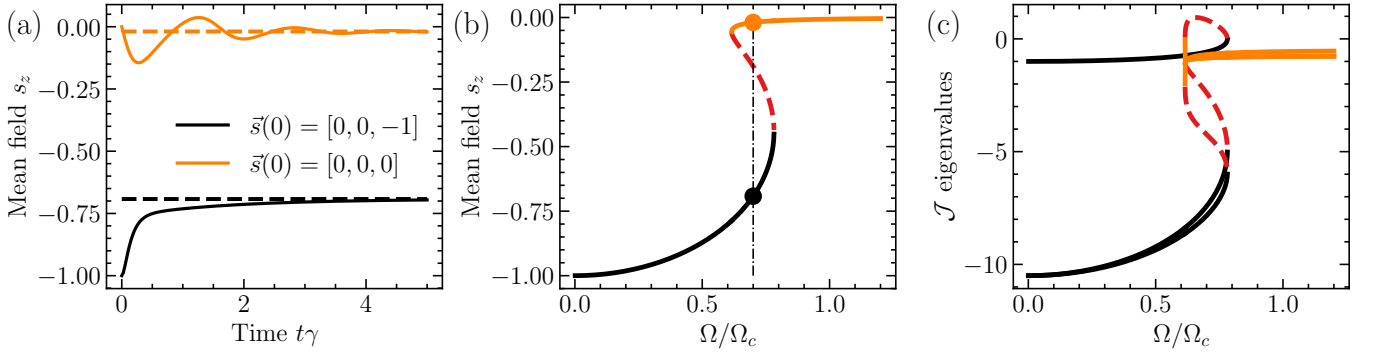


FIG. S2. (a) Numerical time solution of the system (S18) for different initial conditions at $\Omega/\Omega_c = 0.7$ and $\Gamma/\gamma = 20$. (b) The steady states of the system (S18) as function of Ω/Ω_c for $\Gamma/\gamma = 20$. Black and orange solid curves are stable lower and upper branches, and the red dashed curve is an unstable middle branch. (c) Calculated eigenvalues of the Jacobian (S31) for each branch in panel (b).

One can see that the solutions (a) and (b) are real only if $\Omega < \sqrt{2}\Omega_c$, thus imposing restrictions on the perturbative solution in all orders. Substituting Eq. (S25) up to the first order γ to Eq. (S22) we get

$$-2s_z^{(0)}\Gamma - 2(s_z^{(0)})^2\Gamma + 8s_z^{(1)}\Omega^2 + 32s_z^{(0)}s_z^{(1)}\Omega_c^2 + 48(s_z^{(0)})^2s_z^{(1)}\Omega_c^2 = 0. \quad (\text{S28})$$

After the substitution of $s_z^{(0)}$ from the previous step (S27) we find $s_z^{(1)}$

$$s_z^{(1,c)} = 0, \quad s_z^{(1,b)} = \frac{\Gamma}{16\Omega_c^2} \left(1 \mp \sqrt{\frac{1}{1 - 2\Omega^2/\Omega_c^2}} \right). \quad (\text{S29})$$

Repeating this procedure one more time, we get second-order corrections:

$$s_z^{(2,a)} = \pm \frac{\left(\sqrt{\Omega_c^2 - 2\Omega^2} \mp \Omega_c \right) \left(\Gamma^2 \left(\Omega_c \left(\pm \sqrt{\Omega_c^2 - 2\Omega^2} + \Omega_c \right) - \Omega^2 \right) + 16\Omega^2\Omega_c^2 - 8\Omega_c^4 \right)}{128\Omega_c^3 (\Omega_c^2 - 2\Omega^2) \left(\Omega_c \left(\pm \sqrt{\Omega_c^2 - 2\Omega^2} + \Omega_c \right) - 2\Omega^2 \right)}, \quad s_z^{(2,c)} = -\frac{1}{8\Omega^2}. \quad (\text{S30})$$

One can see that $s_z^{(2,c)}$ diverges for small Ω , which is in contradiction with expansion (S25), so this solution works only for big enough values of Ω compared with γ .

In Fig. S1(c), we compare the correction up to second-order with the numerical solution of Eq. (S22) for $\Gamma/\gamma = 50$ and see that solutions (a) and (b) capture lower and middle branches up to $\Omega < \sqrt{2}\Omega_c$, while solution (c) fits the upper branch. The beginning of the bistability region in the numerical solution corresponds to the intersection of solutions (b) and (c).

C. Mean-field time dynamics and stability analysis

As we have shown in the previous section, the system of mean-field equations (S18) has three steady-state solutions in the region of Ω given by Eq. (S24). The stability analysis of these solutions could be performed by calculating the Jacobian matrix \mathcal{J} . From the system of differential equation (S18) we get

$$\mathcal{J} = \begin{bmatrix} -\frac{\gamma}{2} + \frac{\Gamma}{2}s_z & 0 & \frac{\Gamma}{2}s_x \\ 0 & -\frac{\gamma}{2} + \frac{\Gamma}{2}s_z & -2\Omega + \frac{\Gamma}{2}s_y \\ -\Gamma s_x & 2\Omega - \Gamma s_y & -\gamma \end{bmatrix}. \quad (\text{S31})$$

The steady-state point for each Ω is stable if and only if all eigenvalues of the Jacobian matrix \mathcal{J} with substituted steady-state point have real parts that are negative [75]. For the system (S18), it turns out that the lower and upper branches of the mean-field steady-state solution are stable [see Fig. (S2)], whereas the middle branch always has one eigenvalue with a positive real part and therefore is unstable.

For a given value of Γ/γ , one could calculate the eigenvalues of the Jacobian numerically. For each steady-state point, the Jacobian has three eigenvalues. We have substituted the steady-state solution shown in Fig. S2 (b) to the

Jacobian (S31) and calculated the eigenvalues. As seen in Fig. S2 (c), the values from the middle branch [red dashed curve in Fig. S2 (b)] lead to one eigenvalue with real part larger than zero, and therefore the solutions for this branch are unstable.

In the limit case $\Gamma \gg \gamma$, we can show the instability of the middle branch in Fig. S1(a) analytically: for the solution (c) from Eq. (S27) the eigenvalues of (S31)

$$l_1 = -\gamma/2 \quad l_{2,3} = -\frac{1}{4}\left(3\gamma \pm \sqrt{\gamma^2 - 64\Omega^2}\right),$$

always have a negative real part. For the solutions (a) and (b) from (S27) we substitute in (S31) s_y from (S23) expanded up to first order of γ and get

$$l_1 = -\frac{\gamma}{2} + s_z\Gamma, \quad l_2 = \frac{s_z\Gamma}{2} - \gamma\left(\frac{1}{2} + \frac{8\Omega^2}{s_z^2\Gamma^2}\right) + \mathcal{O}(\gamma^2), \quad l_3 = -\gamma\left(1 - \frac{8\Omega^2}{s_z^2\Gamma^2}\right) + \mathcal{O}(\gamma^2).$$

Eigenvalues $l_{1,2}$ are always negative whereas l_3 is positive if we substitute $s_z^{(b)}$ from Eq. (S27) and negative for $s_z^{(a)}$. So the middle branch is unstable for any value of Γ/γ and in the region of Ω given by Eq. (S24), the mean-field has only two stable steady-states. In Fig. S2(a), we demonstrate that both steady states could be reached depending on the initial conditions.

S3. SPIN SQUEEZING

Following the mean-field analysis, we examine the deviations from the mean-field solution to assess atomic correlations in the steady state. We adopt the analytical approach from [31] used for the driven Dicke model with only collective decay and generalize it to the situation where individual decay is also present. Using the Holstein-Primakoff transformation [29, 31, 62], we establish a connection between spin squeezing and bosonic squeezing and calculate the latter analytically.

A. Holstein-Primakoff transformation

Consider the mean-field steady state vector $\langle \hat{\mathbf{S}} \rangle_{\text{MF}} = \frac{N}{2} [0 \ s_y \ s_z]^T$. We rotate the coordinate frame around the x axis so that the new axis z' is along the mean-field direction $\langle \mathbf{S}' \rangle_{\text{MF}} = j_{\text{MF}} [0 \ 0 \ 1]^T$ where we defined the total mean-field spin $j_{\text{MF}} = N\sqrt{s_z^2 + s_y^2}/2$. The new primed mean-field components are related to the initial ones as

$$\begin{bmatrix} s'_x \\ s'_y \\ s'_z \end{bmatrix} = \begin{bmatrix} 1 & 0 & 0 \\ 0 & \cos \theta & -\sin \theta \\ 0 & \sin \theta & \cos \theta \end{bmatrix} \begin{bmatrix} s_x \\ s_y \\ s_z \end{bmatrix}, \quad (\text{S32})$$

where $\theta = \arccos(s_z/\sqrt{s_z^2 + s_y^2})$ and the relations between individual atom operators are given by

$$\begin{bmatrix} \sigma'_n \\ (\sigma'_n)^\dagger \\ (\sigma'_n)^z \end{bmatrix} = \begin{bmatrix} \cos^2 \frac{\theta}{2} & \sin^2 \frac{\theta}{2} & \frac{i}{2} \sin \theta \\ \sin^2 \frac{\theta}{2} & \cos^2 \frac{\theta}{2} & -\frac{i}{2} \sin \theta \\ i \sin \theta & -i \sin \theta & \cos \theta \end{bmatrix} \begin{bmatrix} \hat{\sigma}_n \\ \hat{\sigma}_n^\dagger \\ \hat{\sigma}_n^z \end{bmatrix} \Rightarrow \begin{bmatrix} \hat{\sigma}_n \\ \hat{\sigma}_n^\dagger \\ \hat{\sigma}_n^z \end{bmatrix} = \begin{bmatrix} \cos^2 \frac{\theta}{2} & \sin^2 \frac{\theta}{2} & -\frac{i}{2} \sin \theta \\ \sin^2 \frac{\theta}{2} & \cos^2 \frac{\theta}{2} & \frac{i}{2} \sin \theta \\ -i \sin \theta & i \sin \theta & \cos \theta \end{bmatrix} \begin{bmatrix} \sigma'_n \\ (\sigma'_n)^\dagger \\ (\sigma'_n)^z \end{bmatrix}. \quad (\text{S33})$$

Within the primed frame, we now use the Holstein-Primakoff transformation to account for small spin fluctuations around the mean spin directed at z' . Typically, as in the Dicke problem [31], the Holstein-Primakoff transformation is performed on collective variables:

$$S'_+ = \sum_n (\sigma'_n)^\dagger \rightarrow \sqrt{2j_{\text{MF}}} \hat{b} + \mathcal{O}\left(\frac{1}{j_{\text{MF}}}\right), \quad S'_- = \sum_n \sigma'_n \rightarrow \sqrt{2j_{\text{MF}}} \hat{b}^\dagger + \mathcal{O}\left(\frac{1}{j_{\text{MF}}}\right), \quad (\text{S34a})$$

$$S'_z \rightarrow j_{\text{MF}} + \mathcal{O}\left(\frac{1}{j_{\text{MF}}}\right). \quad (\text{S34b})$$

Here \hat{b} and \hat{b}^\dagger are bosonic ladder operators, satisfying $[\hat{b}, \hat{b}^\dagger] = 1$, that represent small spin fluctuations for $j_{\text{MF}} \gg 1$. In our case, where individual decay γ_F and related noise $\hat{\eta}_n$ for each atom are present, the summation of Eqs. (S13)-(S14) could not be rewritten in terms of collective operators used in Eqs. (S34). Therefore, to describe our system using bosonic operators, we must introduce the local bosonic operators for each atom n \hat{a}_n and \hat{a}_n^\dagger with $[\hat{a}_n, \hat{a}_m^\dagger] = \delta_{nm}$. Based on Eq. (S34b) we substitute

$$(\sigma'_n)^z \rightarrow 2j_{\text{MF}}/N, \quad (\text{S35a})$$

and then, for the commutation relation $[(\sigma'_n)^\dagger, \sigma'_n] = (\sigma'_n)^z$ to hold, we set

$$\sigma'_n = \sqrt{2j_{\text{MF}}/N} \hat{a}_n^\dagger, \quad (\sigma'_n)^\dagger = \sqrt{2j_{\text{MF}}/N} \hat{a}_n. \quad (\text{S35b})$$

To find an equation of motion for the spin fluctuations \hat{a}_n we use (S33)

$$\frac{d(\sigma'_n)^\dagger}{dt} = \sin^2 \frac{\theta}{2} \dot{\hat{\sigma}}_n + \cos^2 \frac{\theta}{2} \dot{\hat{\sigma}}_n^\dagger - \frac{i}{2} \sin \theta \dot{\hat{\sigma}}_n^z, \quad (\text{S36})$$

and then substitute Eqs. (S13)-(S14). Then, we apply the transformation (S35) and neglect terms of second order in the fluctuations, $\hat{a}_n \hat{\xi}_n$, $\hat{a}_n^\dagger \hat{\xi}_n$, $\hat{a}_n \hat{a}_m$, $\hat{a}_n \hat{a}_m^\dagger$, $\hat{a}_n \hat{f}$, $\hat{a}_n^\dagger \hat{f}$, obtaining the linearized Heisenberg-Langevin equation

$$\dot{\hat{a}}_n = \frac{\gamma_{1D} j_{\text{MF}}}{N} \cos \theta \sum_{m \neq n} \hat{a}_m - \frac{\gamma}{2} \hat{a}_n - \frac{\gamma}{4} \sin^2 \theta (\hat{a}_n - \hat{a}_n^\dagger) + \sqrt{\frac{j_{\text{MF}}}{2N}} \left[\cos \theta (\hat{f} + \hat{f}^\dagger + \hat{\eta}_n + \hat{\eta}_n^\dagger) + (\hat{f}^\dagger - \hat{f} + \hat{\eta}_n^\dagger - \hat{\eta}_n) \right]. \quad (\text{S37})$$

Next, we introduce the collective bosonic operator $\hat{a} = \frac{1}{\sqrt{N}} \sum_n \hat{a}_n$ and sum Eq. (S37) over n , finding

$$\dot{\hat{a}} = \frac{\Gamma j_{\text{MF}} \cos \theta}{N} \hat{a} - \frac{\gamma}{2} \hat{a} - \frac{\gamma}{4} \sin^2 \theta (\hat{a} - \hat{a}^\dagger) + \sqrt{\frac{j_{\text{MF}}}{2N}} \left[\cos \theta (\hat{F} + \hat{F}^\dagger + \hat{\eta} + \hat{\eta}^\dagger) + (\hat{F}^\dagger - \hat{F} + \hat{\eta}^\dagger - \hat{\eta}) \right], \quad (\text{S38})$$

where $\hat{\eta} = \frac{1}{\sqrt{N}} \sum_n \hat{\eta}_n$ and $\hat{F} = \sqrt{N} \hat{f}$. Finally, solving Eq. (S38) as a system of equations for \hat{a} and \hat{a}^\dagger in steady state, $t \gg [\Gamma \cos(\theta) + \gamma]^{-1}$, we obtain

$$\hat{a}(t) = \sqrt{\frac{j_{\text{MF}}}{2N}} \int_0^t dt' \exp \left[\left(-\Gamma j_{\text{MF}} \cos \theta / N + \frac{\gamma}{2} \right) (t' - t) \right] \left\{ \left(\hat{F}(t') + \hat{\eta}(t') \right) \left(\cos \theta - \exp \left[\frac{\gamma}{2} \sin^2 \theta (t' - t) \right] \right) + \left(\hat{F}^\dagger(t') + \hat{\eta}^\dagger(t') \right) \left(\cos \theta + \exp \left[\frac{\gamma}{2} \sin^2 \theta (t' - t) \right] \right) \right\}. \quad (\text{S39})$$

B. Spin squeezing

The spin squeezing parameter is given by $\xi^2 = \min_\varphi \text{Var}[\hat{S}'_\varphi] N / |\langle \hat{\mathbf{S}} \rangle|^2$, recalling that \hat{S}'_φ is the spin vector component perpendicular to the mean-spin direction. Therefore, in terms of the primed frame from Eqs. (S33) and (S35), we have

$$\hat{S}'_\varphi = \frac{e^{i\varphi} \sum_n \sigma'_n + e^{-i\varphi} \sum_n (\sigma'_n)^\dagger}{2} = \sqrt{\frac{j_{\text{MF}}}{2N}} (e^{i\varphi} \hat{a}^\dagger + e^{-i\varphi} \hat{a}). \quad (\text{S40})$$

Moreover, considering the mean spin $|\langle \hat{\mathbf{S}} \rangle|^2 = N^2 (s_z^2 + s_y^2) / 4 = j_{\text{MF}}^2$, the spin squeezing parameter is then simply given by

$$\xi^2 = \min_\varphi \text{Var}[e^{i\varphi} \hat{a}^\dagger + e^{-i\varphi} \hat{a}] = 1 + 2 \langle \hat{a}^\dagger \hat{a} \rangle - 2 |\langle \hat{a} \rangle|^2. \quad (\text{S41})$$

The required correlators of \hat{a} are then obtained from the solution (S39) as

$$\langle \hat{a}^\dagger \hat{a} \rangle = \frac{(\gamma + \Gamma) |\mathbf{s}|}{4} \left[\frac{1}{-\Gamma |\mathbf{s}| \cos \theta + \gamma(1 + \sin^2 \theta)} + \frac{2 \cos \theta}{-\Gamma |\mathbf{s}| \cos \theta + \gamma(1 + \sin^2 \theta/2)} + \frac{\cos^2 \theta}{-\Gamma |\mathbf{s}| \cos \theta + \gamma} \right], \quad (\text{S42a})$$

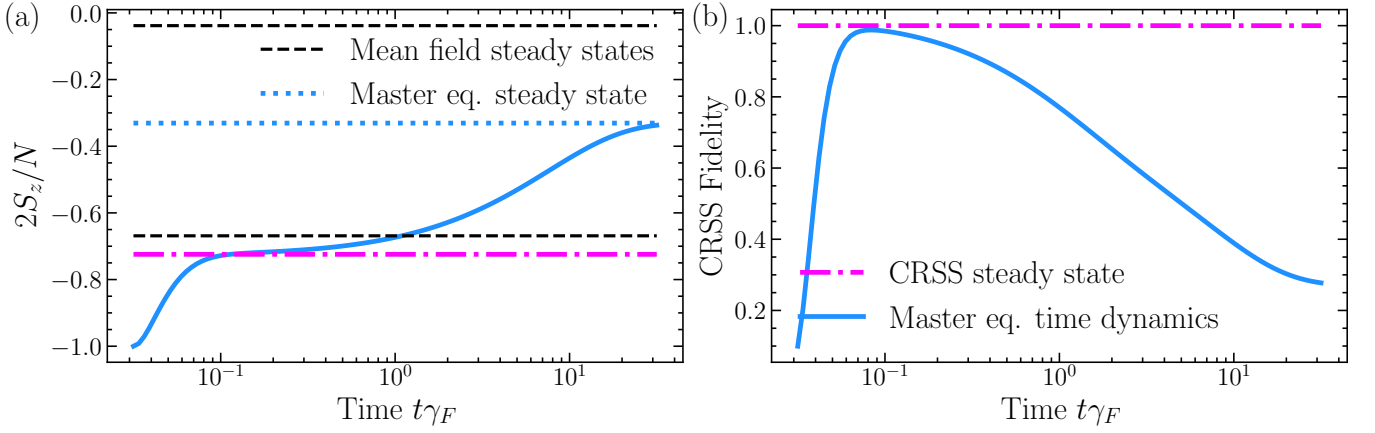


FIG. S3. (a) \hat{S}_z time dynamics and (b) CRSS fidelity from the solution of the master equation (S15) (blue solid curve); Master equation \hat{S}_z steady state (blue dotted curve); Mean-field stable steady states from the numerical solution of Eq. (S22) (black dashed curves) and CRSS steady state (S21) (magenta dot-dashed curve). Parameters $N = 18$, $\Omega/\Omega_c = 0.73$, $\Gamma/\gamma = 15.5$.

$$\langle \hat{a}^2 \rangle = \frac{(\gamma + \Gamma)|\mathbf{s}|}{4} \left[\frac{\cos^2 \theta}{-\Gamma|\mathbf{s}| \cos \theta + \gamma} - \frac{1}{-\Gamma|\mathbf{s}| \cos \theta + \gamma(\sin^2 \theta + 1)} \right], \quad (\text{S42b})$$

where we introduced $|\mathbf{s}| = 2j_{\text{MF}}/N = \sqrt{s_z^2 + s_y^2}$ and used the Langevin-noise correlators derived from Eqs. (S11) and (S12)

$$\langle \hat{F}(t') \hat{F}^\dagger(t'') \rangle = N\gamma_{1D} \delta(t' - t''), \quad \langle \eta(t') \eta^\dagger(t'') \rangle = \gamma_F \delta(t' - t''). \quad (\text{S43})$$

Now, we consider spin squeezing in some limiting cases. First of all, if in Eqs. (S42) we set γ to be equal zero and substitute the solution Eq. (S21), we get the squeezing in the Dicke model for $N \rightarrow \infty$ [22, 29, 31]

$$\xi^2 = -\cos \theta = \sqrt{1 - \frac{\Omega^2}{\Omega_c^2}}, \quad (\text{S44})$$

where we found θ from the analytical expression (S21). When γ_F is considered, we have two stable branches in the bistable region shown in Fig. S2(b). However, Eq. (S42) is derived assuming that $j_{\text{MF}} \gg 1$, which holds only for the lower branch [black solid line in Fig. S2(b)]. For example, the spin squeezing obtained by substituting into Eqs. (S41) and (S42) the lower-branch mean-field solution obtained numerically from Eq. (S22) for $\Gamma/\gamma = 15.5$ is shown in Fig. 2(c) of the main text and exhibits excellent agreement with the exact numerical result, obtained directly from the density matrix solution of the master equation [Eq. (1) of the main text]. This holds for the relevant regime wherein $\langle \hat{S}_z \rangle$ coincides with the mean-field lower branch solution. More insights follow from the comparison with the squeezing calculated on ρ_+ , corresponding to the mean-field lower branch density matrix from the spectral decomposition. It agrees with analytics almost until the end of the bistability region [Fig. 3(d) in the main text].

In the limiting case $\Gamma \gg \gamma \neq 0$ we still have $\xi^2 = -\cos \theta$, but now we substitute θ from $s_z^{(0,a)}$ from (S27):

$$\xi^2 = \frac{1 + \sqrt{1 - 2\Omega^2/\Omega_c^2}}{\sqrt{2}\sqrt{1 + \Omega^2/\Omega_c^2} + \sqrt{1 - 2\Omega^2/\Omega_c^2}}. \quad (\text{S45})$$

This result is valid in the region $\Omega \leq \Omega_c/\sqrt{2}$ wherein the lower-branch solution is relevant. Since the squeezing parameter ξ^2 decreases with Ω it thus obtains its optimal (minimal) value $1/\sqrt{3}$ at $\Omega = \Omega_c/\sqrt{2}$.

54. ADDITIONAL MASTER EQUATION RESULTS

A. Time dynamics

The time dynamics of the observable \hat{S}_z for a specific drive value Ω obtained from the numerical solution of the master equation (S15) is shown in Fig. S3(a). On long enough times $t\gamma_F \approx 10^2$ it reaches the steady state value. As

can be seen from the mean-field system of equations (S18), at short times, the solution reaches \hat{S}^2 -conserved steady state given by (S21) and the true master equation solution stays close to the steady state (S21) for a time $\sim 1/\gamma_F$.

To prove that not only the \hat{S}_z observable but the whole density matrix is close to the Dicke \hat{S}^2 -conserved steady state in Fig. S3(b), we show the fidelity of the density matrix with the coherently radiating spin state (CRSS) that is the asymptotical pure steady state of this model [22]. One can see that in the same region where the \hat{S}_z expectation value is close to the (S21), this fidelity does not get below 0.8 and reaches unity at some point.

B. Density matrix peaks width

In Fig. S4 we show the probability distribution for observing an eigenvalue m of \hat{S}_z , $P_m = \sum_{j=|m|}^{N/2} \langle j, m | \rho_s | j, m \rangle$ for different values of drive Ω and number of atoms N . The general theory built in the main text suggests that these two peaks correspond to the states between which we observe quantum jumps. Their width is related to the fluctuations observed in Fig. 4 in the main text, and relative height is the relation between the time the system spends on each state in one trajectory.

We note that the peaks become narrower with increasing the amount of the atoms N , allowing us to expect less fluctuations in the trajectories for larger N than shown in Fig. 4 of the main text and the peaks maximums excellently agree with the mean-field steady states from Eq. (S22).

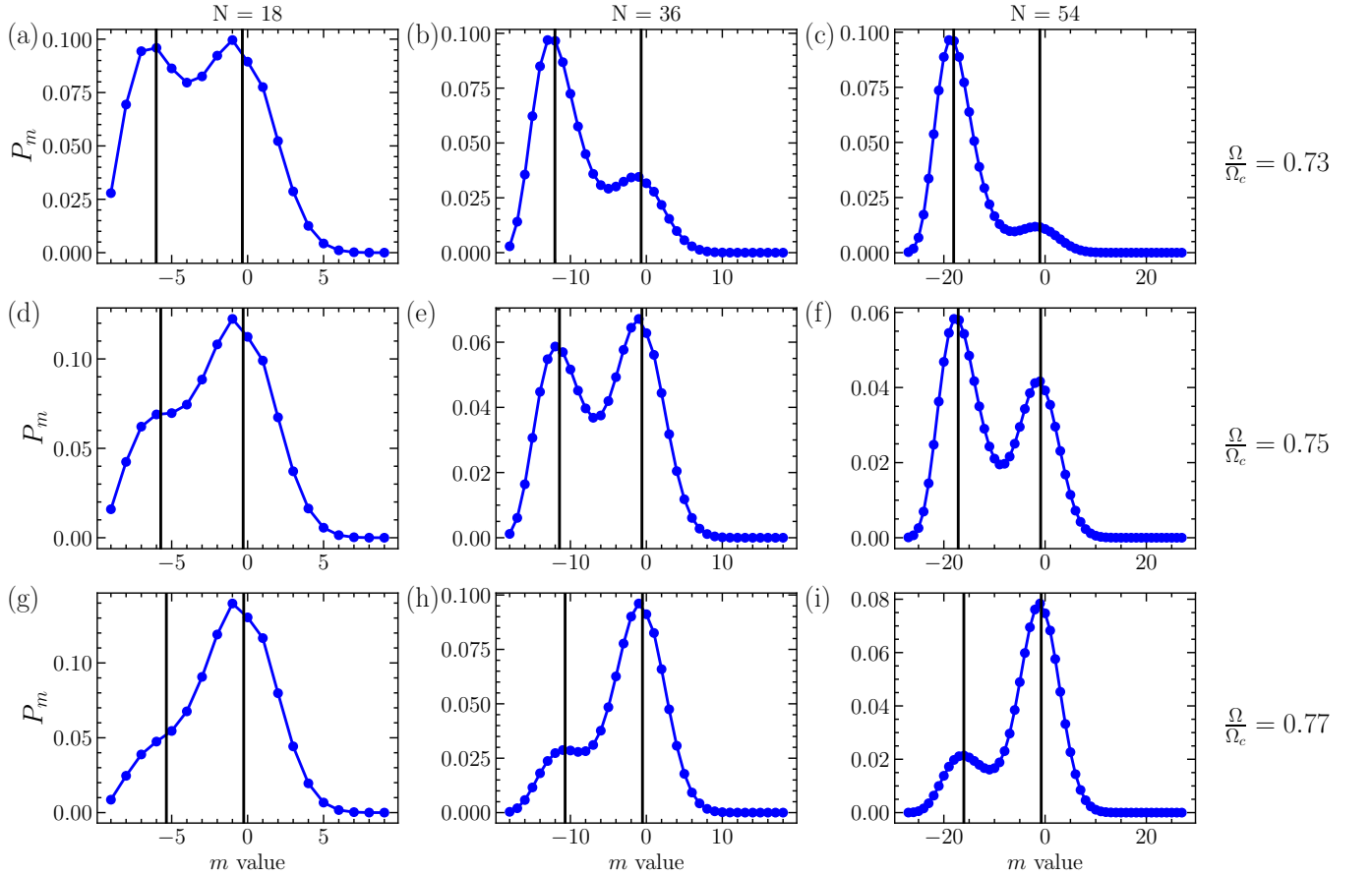


FIG. S4. P_m distribution at $\Gamma/\gamma = 15.5$ for different numbers of atoms (columns) and different drive values (rows). Black curves are the mean-field solutions from Eq. (S22).